Research Update: Spin transfer torques in permalloy on monolayer MoS_2

Wei Zhang,[1,a] Joseph Sklenar,[1,2,a] Bo Hsu,[3] Wanjun Jiang,[1] Matthias B. Jungfleisch,[1] Jiao Xiao,[3] Frank Y. Fradin,[1] Yaohua Liu,[4] John E. Pearson,[1] John B. Ketterson,[2] Zheng Yang,[3,b] and Axel Hoffmann[1,c]

[1]*Materials Science Division, Argonne National Laboratory, Lemont, Illinois 60439, USA*
[2]*Department of Physics and Astronomy, Northwestern University, Evanston, Illinois 60208, USA*
[3]*Department of Electrical and Computer Engineering, University of Illinois at Chicago, Chicago, Illinois 60607, USA*
[4]*Quantum Condensed Matter Division, Oak Ridge National Laboratory, Oak Ridge, Tennessee 37831, USA*

(Received 1 December 2015; accepted 17 February 2016; published online 3 March 2016)

We observe current induced spin transfer torque resonance in permalloy (Py) grown on monolayer MoS_2. By passing rf current through the Py/MoS_2 bilayer, field-like and damping-like torques are induced which excite the ferromagnetic resonance of Py. The signals are detected via a homodyne voltage from anisotropic magnetoresistance of Py. In comparison to other bilayer systems with strong spin-orbit torques, the monolayer MoS_2 cannot provide bulk spin Hall effects and thus indicates the purely interfacial nature of the spin transfer torques. Therefore our results indicate the potential of two-dimensional transition-metal dichalcogenide for the use of interfacial spin-orbitronics applications. © *2016 Author(s). All article content, except where otherwise noted, is licensed under a Creative Commons Attribution 3.0 Unported License.* [http://dx.doi.org/10.1063/1.4943076]

The development of efficient mechanisms for reorienting magnetization using the least possible power is the key to modern magnetic memory and logic devices.[1] One promising approach is to use spin-orbit interactions (SOIs) in heavy metal/ferromagnet bilayers[2,3] which can yield strong current-driven torques acting on the magnetic layer, via the spin Hall effect (SHE)[4–7] of the heavy metal or other interface spin-orbit effects[8] such as the Rashba-Edelstein effect (REE).[9–16] Due to the transverse nature of these spin transport phenomena, the efficiency of the spin current generation generically increases as the cross section of the charge current carrying layer is reduced.[5] This motivates the search for two-dimensional (2D) systems as a source for spin current. Interestingly, as part of the search for materials to provide more efficient current-induced torques, recent experiments have demonstrated large spin-orbit torques in topological insulators (TIs),[17,18] due to the fact that an electron's spin orientation is locked relative to its propagation direction in the surface states of TIs. Such spin-momentum locking gives rise to a non-equilibrium surface spin accumulation while flowing a charge current. If this spin accumulation couples to an adjacent magnetic film, the resulting flow of spin angular momentum will exert a spin-transfer torque on the magnet.

Another possible pathway towards spin transfer torques with 2D systems is given by the transition metal dichalcogenide (TMD) family of materials, which has attracted increased attention in the nanoelectronics community due to their layered structure, enabling readily the preparation of individual monolayers. However, much of the community's interest in TMDs has been focused on transistor technology, while less work has been done with respect to their potential in spintronics applications.

[a]W. Zhang and J. Sklenar contributed equally to this work.
[b]Electronic mail: yangzhen@uic.edu.
[c]Electronic mail: hoffmann@anl.gov.

 ©Author(s) 2016

Reuse of AIP Publishing content is subject to the terms at: https://publishing.aip.org/authors/rights-and-permissions. IP: 128.219.49.13 On: Fri, 04 Mar 2016 15:43:43

Actually, one of the appealing features of many TMDs is the spin splitting (either Rashba[19,20] or Zeeman type[21]) at the surface due to the broken inversion symmetry, which also gives rise to spin-momentum locking and therefore potentially large spin-orbit torques once coupled to a ferromagnet. In addition, a recent rise in the interest of metallic TMDs (e.g., TaS_2 and $TaSe_2$)[22] points towards new opportunities for combining Rashba torques with spin Hall torques by flowing large density of charge current in the TMDs themselves. Due to the large intrinsic SOI of the heavy elements, large SHE and REE are also conceivable in their TMDs.[23] In this work, we investigate any possible spin-torques in permalloy(Py, $Ni_{80}Fe_{20}$)/MoS_2 heterostructures by using the spin-torque ferromagnetic resonance (ST-FMR) approach.[3]

The MoS_2 nanosheets were grown on SiO_2 (300 nm)-on-Si substrates using a home-built chemical vapor deposition system. MoO_3 and S were used as the source materials. Ar gas was used as the carrier gas with a flow rate of 50 SCCM during growth. The growth temperature, pressure, and time were 875 °C, ~8 Torr, and 5 min, respectively. Single-crystalline MoS_2 monolayers in triangle-shape with size up to several tens of μm were selected for this study. The as-grown MoS_2 flakes in their monolayer form were subsequently characterized by optical microscopy, scanning electron microscopy, atomic force microscopy (AFM), and Raman spectroscopy (see Fig. 1). An optical microscopy image of a representative as-grown MoS_2 sample is shown in Fig. 1(a), and Fig. 1(b) shows a

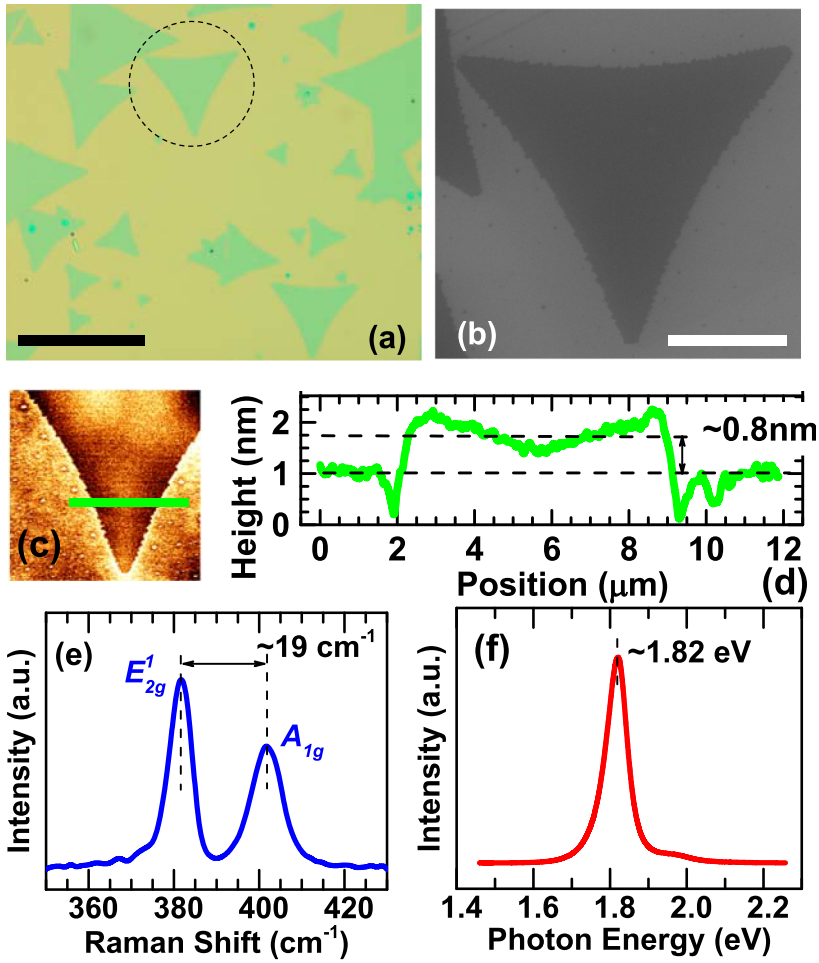

FIG. 1. (a) Optical microscopy image of a MoS_2 sample. The scale bar in the image is 40 μm. (b) Scanning electron microscopy image of a triangular single-crystalline MoS_2 monolayer [dashed-line-circled region in (a)]. The scale bar in the image is 10 μm. (c) Atomic force microscopy image of the same MoS_2 monolayer shown in (b). The size of the AFM image is 20 μm×20 μm. (d) Height-profile scan along the green line in (c). (e) Raman spectrum of the MoS_2 monolayer shown in (b) and (c). (f) Photoluminescence spectrum of the MoS_2 monolayer shown in (b) and (c).

Reuse of AIP Publishing content is subject to the terms at: https://publishing.aip.org/authors/rights-and-permissions. IP: 128.219.49.13 On: Fri, 04 Mar 2016 15:43:43

corresponding scanning electron microscopy image of a triangular single-crystalline MoS_2 monolayer. Figure 1(c) shows the AFM image of the same MoS_2 monolayer shown in Fig. 1(b). A corresponding AFM height-profile scan along the green line in Fig. 1(c) is shown in Fig. 1(d). The measured thickness of the MoS_2 nanoflake is ~0.8 nm, which is consistent with the thickness of monolayer MoS_2. Figure 1(e) shows the Raman spectrum of the MoS_2 monolayer shown in Figs. 1(b) and 1(c). The distance between the E^1_{2g} and A_{1g} peaks in the Raman spectrum is ~19 cm^{-1}, indicating the monolayer nature of the MoS_2. Figure 1(f) shows the photoluminescence (PL) spectrum of the MoS_2 monolayer shown in Figs. 1(b) and 1(c). The PL spectrum shows strong emission with the peak position located at ~1.82 eV, again confirming the monolayer nature of the MoS_2.

To fabricate the devices, we deposit the Py layers using magnetron sputtering or e-beam evaporation on individual monolayer flakes of MoS_2. The different approaches of Py deposition allow us to exclude possible fabrication-induced artifacts from our measurements. The thickness of the Py layers is 5 nm. During sputtering, the substrate is kept well-separated from the target and the deposition rate is kept < 1 Å/s in order to avoid damage to the MoS_2 layer. The Py layers, in the shape of 30-μm-long and 5-μm-wide strips, as well as the subsequent electrical contacts were patterned by photolithography. Specifically, we patterned the Py layer using optical lithography and liftoff, with electrical contacts made from 3 nm Ti/120 nm Au in a symmetric geometry [Fig. 2(b)], so that when the samples are contacted using a ground-signal-ground (G-S-G) high-frequency probe, the currents flowing in the contacts produce almost no net Oersted field acting on the sample. In the study by Mellnik *et al.* on Py/TI bilayers, the resistivity of the Bi_2Se_3 is far larger than that of Py so that the great majority of the current is shunted through the Py; nevertheless they measured strong enough spin torque signals from the Bi_2Se_3 surface states. This shunting effect is less an issue in our case due to the "monolayer" nature of MoS_2, i.e., there are no bulk states but only a Py/MoS_2 interface gives rise to the spin to charge conversion.

We determine the strength of current-induced torque with the ST-FMR technique developed previously to measure the spin Hall torque from heavy metals.[2,3] Using the circuit shown in Fig. 2, we apply a microwave current with fixed frequency and sweep an in-plane magnetic field through the ferromagnetic resonance condition of Py. The oscillating current-induced torques cause the Py magnetization to precess, yielding resistance oscillations on account of the anisotropic magnetoresistance (AMR) of Py. This generates a direct voltage, V_{dc}, that results from mixing between the applied alternating current and the oscillating resistance. The two vector components of the current-induced torque, in the $\hat{\mathbf{m}} \times (\hat{y} \times \hat{\mathbf{m}})$ (||, "in-plane") and $(\hat{y} \times \hat{\mathbf{m}})$ ($\perp$, "perpendicular") directions, with $\hat{\mathbf{m}}$ being the unit vector of the magnetization direction, can be obtained from the amplitudes of the symmetric and antisymmetric components of the resonance lineshapes. We performed ST-FMR experiments for two device geometries, one with normal rectangular electrical contacts that we contact to external electronics using wire bonding; this device geometry is compatible with an existing sample holder that allows for both in-plane and out-of-plane ST-FMR experiments. The other geometry is based on coplanar-waveguide (CPW)-like electrical contacts (see Fig. 2) that are connected to using low-loss

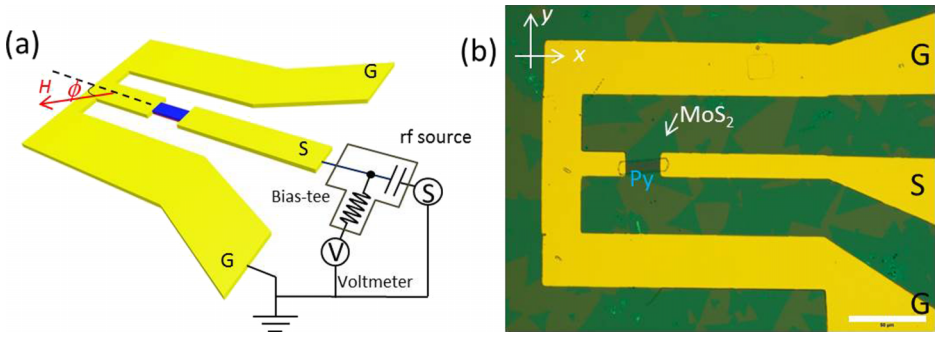

FIG. 2. (a) Schematic illustration of the spin torque FMR experimental setup [S: signal line; G: ground line]. (b) Photoimage of ST-FMR device consisting a Py layer (5 nm) on a monolayer MoS_2. The Py strip is patterned into a 30 μm×5 μm rectangle. An external magnetic field is applied along 45° with respect to the sample long axis (current direction). (Scale bar: 50 μm.)

Reuse of AIP Publishing content is subject to the terms at: https://publishing.aip.org/authors/rights-and-permissions. IP: 128.219.49.13 On: Fri, 04 Mar 2016 15:43:43

rf probes in a probe station. For both geometries, the core component of the devices is the same, i.e., 30 μm × 5 μm Py microstrips deposited on top of individual monolayer flakes of MoS_2.

Before showing the results from the two geometries, we discuss the model for their analysis in more detail. To model both a field-like and an anti-damping-like drive torque, the magnetization equation of motion can be written as

$$\frac{d\hat{\mathbf{m}}}{dt} = -\gamma\hat{\mathbf{m}} \times H + \alpha\hat{\mathbf{m}} \times \frac{d\hat{\mathbf{m}}}{dt} + \gamma\tau_{\perp}\hat{\mathbf{m}} \times \hat{y} + \gamma\tau_{\parallel}\hat{\mathbf{m}} \times (\hat{y} \times \hat{\mathbf{m}}), \tag{1}$$

while $\tau_\perp$ is the magnitude of the effective field applying the field-like torque and $\tau_\parallel$ is the magnitude of the field applying the anti-damping-like torque. Both $\tau_\perp$ and $\tau_\parallel$ have amplitudes that are oscillatory at the microwave drive frequency ω. The gyromagnetic ratio is γ and the Gilbert damping parameter is α. Note that Eq. (1) assumes only a spin accumulation along the y-axis, i.e., in the interfacial plane. Given that a monolayer of MoS_2 has no inversion symmetry even for in-plane directions, it is conceivable that there could also be a spin accumulation along the z-axis, i.e., perpendicular to the interface.[24] However, when studying the in-plane angular dependence of the dc lineshape, the symmetric and antisymmetric amplitudes can be fit to a $\cos\phi \sin 2\phi$ function. This angular dependence suggests that the rectification is occurring from the well-know phenomenon of the AMR of the Py mixing on resonance with the microwaves[25,26] and that the spin transfer torques only originate from spin accumulations polarized along the y-axis. If AMR rectification is the mechanism for the dc voltage, the following equation can be used to describe the in-plane angular dependence of the resonance that is driven by the $\tau_\perp$ and $\tau_\parallel$ torques:

$$V_{DC} \propto \frac{\partial R}{\partial \phi} \cos\phi[F_A\tau_{\perp}(B_{\circ} + 4\pi M_{eff}) + F_S\tau_{\parallel}\omega\Delta]. \tag{2}$$

For Py, $\frac{\partial R}{\partial \phi} \sim \sin 2\phi$. The FMR resonance frequency is given as $\omega_{\circ} = \gamma\sqrt{B_{\circ}(B_{\circ} + 4\pi M_{eff})}$. $B_\circ$ is the experimental applied field and M_{eff} is the effective saturation magnetization of the material. The function $F_S = 1/[(\omega^2 - \omega_o^2)^2 + \Delta^2]$ is a symmetric lineshape and F_A is the antisymmetric lineshape function that is written as $F_A = (\omega^2 - \omega_o^2)F_S$. Finally, $\Delta = \gamma\omega\alpha(2B_{\circ} + 4\pi M_{eff})$.

To begin with, we describe the results from the CPW-like devices where the Py is sputtered on top of MoS_2. Figure 3(a) shows the results of the ST-FMR measurement for a 30 μm × 5 μm device with CPW-like contacts and with an in-plane magnetic field oriented $\phi = 45°$ relative to the current. Under a field reversal, the sign change of both the symmetric and antisymmetric amplitude components of the line shape agrees with the spin-torque picture. Figure 3(b) compares the voltage of this Py/MoS_2 bilayer and a pure Py layer measured at the same condition. For the pure Py sample, a small dc voltage in the shape of an antisymmetric Lorentzian resonance is observed. Past experiments have suggested that this small voltage is due to a non-uniform current density in the Py that can lead to a self-induced precession of the magnetization.[3] Regardless, both symmetric and antisymmetric voltage components increase significantly for the Py/MoS_2 bilayer. We also performed ST-FMR measurements at different in-plane field orientations (ϕ), both the symmetric and antisymmetric components of V_{dc} on ϕ are in good agreement with the $\cos\phi \sin 2\phi$ behavior [Figs. 3(c) and 3(d)].

We then investigated the frequency and power dependence of the torque ratio using the CPW-like devices. We first extract the torque ratio at a fixed power of 15 dBm from 4 to 7 GHz for one sample using the fitting shown in Fig. 4(c). A Kittel fitting to the FMR resonance fields, as shown in Fig. 4(b), yields an effective magnetization of Py, $M_{eff} = 509.6 \pm 7.3$ kA m^{-1}, which is less than its bulk value. We use a value of $dR/d\phi = 1.284\ \Omega$/rad extracted from an experimental measurement of the in-plane angular derivative of the magnetoresistance shown in Fig. 4(a). We also measure the lineshapes at a variety of power from 8 to 17 dBm and at a fixed frequency 4 GHz, Fig. 4(d). Figures 4(e) and 4(f) summarize the dependences of $\tau_\perp/\tau_\parallel$ on the frequency and the power, respectively. As expected, we observe no appreciable dependence of $\tau_\perp/\tau_\parallel$ as a function of either frequency or power. Averaging the values for both frequency- and power-data, we conclude that $|\tau_\perp/\tau_\parallel| = 0.19 \pm 0.01$ in our Py/MoS_2 bilayer system.

A more comprehensive angular dependent study was conducted on the "normal-contacts" devices where the Py is e-beam evaporated on top of MoS_2. Figure 5(a) shows the coordinate system that was adopted for the applied field configuration in the Py film. In addition to the azimuthal angle, ϕ, two

Reuse of AIP Publishing content is subject to the terms at: https://publishing.aip.org/authors/rights-and-permissions. IP: 128.219.49.13 On: Fri, 04 Mar 2016 15:43:43

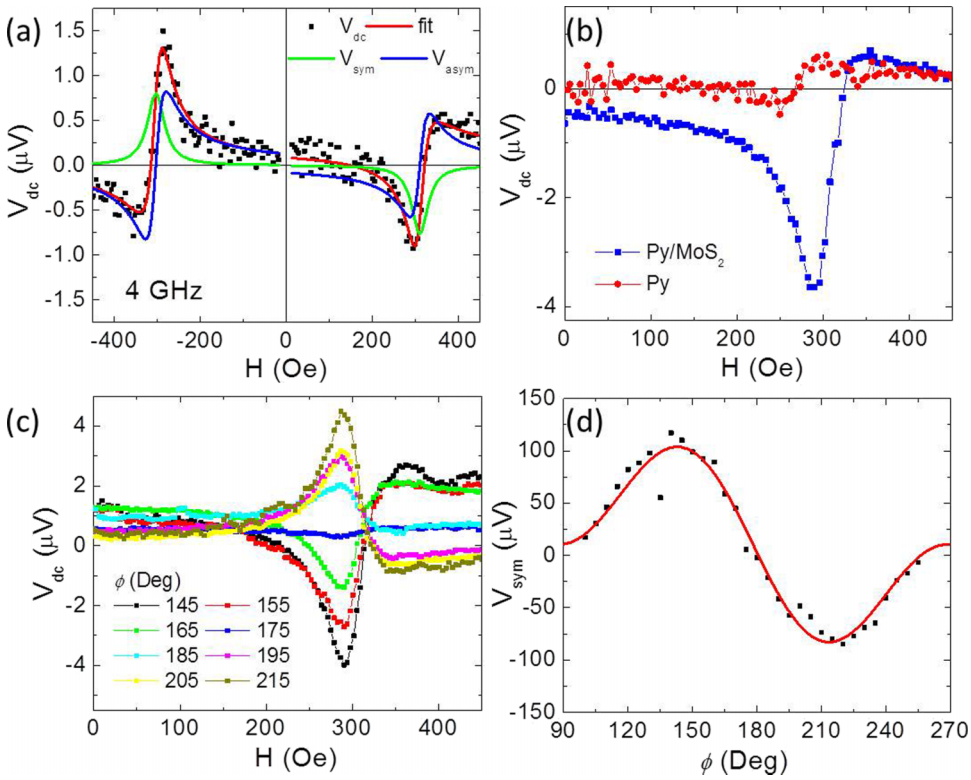

FIG. 3. Measurements with sputtered Py on MoS_2 and CPW-like contacts. (a) Bi-polar field scan of ST-FMR signals. (b) Comparison of the V_{dc} signals measured for a Py/MoS_2 and for a pure Py. (c) V_{dc} signals measured at selective field angles, ϕ. (d) ϕ-dependence of the symmetric voltage component V_{sym} and the corresponding theoretical fitting by $\cos(\phi)\sin(2\phi)$.

polar angles are introduced: θ is the polar angle from off the normal, z-axis, at which the external field is applied; ψ is another polar angle that corresponds to the direction of the magnetization. In Figs. 5(c) and 5(d), the θ dependence and a subset of the ϕ angular dependence of the ST-FMR lineshape are, respectively, shown. For this set of experiments, ω was held fixed at 5.5 GHz. For this "normal-contact" device, a reference sample of a Ti/Py bilayer was fabricated. An ST-FMR trace near $\phi = 45°$ is shown in Fig. 5(b) comparing the reference sample to the MoS_2/Py bilayer.

The complete in-plane ϕ dependence of the symmetric and antisymmetric amplitudes of the ST-FMR signal is shown in Figs. 6(a) and 6(b), respectively. The symmetric and antisymmetric amplitudes are both fit to a $\cos\phi \sin 2\phi$ function. This angular dependence again suggests that the rectification is occurring from the well-know phenomenon of the AMR of the Py mixing on resonance with the microwaves. By fitting the ratio of the symmetric and antisymmetric components of the lineshape, the ratio of the two driving torques was calculated from the in-plane data. For our MoS_2/Py bilayer on the "normal-contact" device, we found $\tau_\perp/\tau_\parallel = 0.08 \pm 0.01$. The in-plane measurements for both the CPW-like and "normal-contact" devices *show very large anti-damping-like torques* as evidenced by the large symmetric voltages. The observed large spin torques from both types of devices with different Py growth techniques support the fact that the spin torque is an intrinsic property of MoS_2/Py interface rather than fabrication induced artifacts.[27]

Typically, when ST-FMR measurements are used to measure anti-damping-like torques driven by the spin Hall effect, the torque ratio is converted to a spin Hall angle. It is not straightforward to perform such a conversion here given that the MoS_2 layer is a single monolayer. We do note that the torque ratios calculated from the two different device geometries and Py growth show a modest quantitative difference. One explanation is that the different device geometries may lead to differences in the phase of the driving current to the respective torques. Phase shifts have been shown both experimentally[28] and theoretically,[29] to effect lineshapes in ST-FMR experiments. There is good evidence that rules out phase shifts as evidenced by the two reference samples, both of which mainly show

Reuse of AIP Publishing content is subject to the terms at: https://publishing.aip.org/authors/rights-and-permissions. IP: 128.219.49.13 On: Fri, 04 Mar 2016 15:43:43

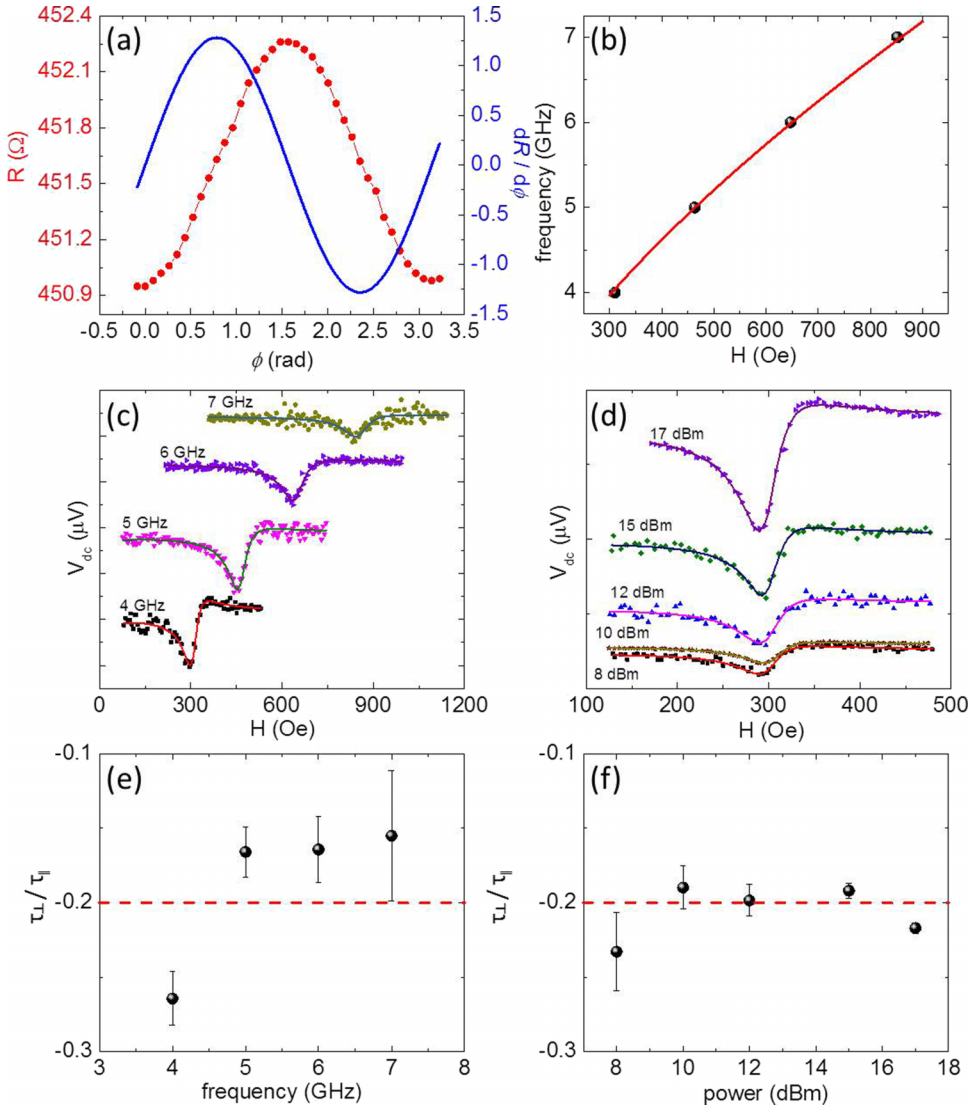

FIG. 4. Measurements with sputtered Py on MoS_2 and CPW-like contacts. (a) ϕ-dependence of the device anisotropic magnetoresistance (R) and its derivative $dR/d\phi$, measured at 3 kOe external field. (b) Kittel fitting of the FMR resonance conditions. ST-FMR spectra measured (c) at different frequencies and at fixed power of 10 dBm for one device and (d) at different power values and at fixed frequency of 4 GHz for another device. (e) and (f) summarize the frequency- and power-dependence of the ratio between the two torques, $\tau_\perp/\tau_\parallel$, which is extracted by Eq. (2) using the symmetric and antisymmetric Lorentzian signals. A red dashed line is drawn at a value of 0.2.

small *asymmetric* amplitudes. Both reference samples should be driven only by a field-like, $\tau_\perp$ torque. As shown in Eq. (2), an equation that does not include phase shifts, a $\tau_\perp$ torque by itself produces only an antisymmetric signal. Another possible explanation is simply that the patterning of the Py bar onto the MoS_2 flake is sensitive to variables such as the relative orientation between the Py bar and the crystallographic axes of MoS_2 single-crystal. Lastly, it is possible that the magnitude of the spin transfer torque may depend on interfacial quality, which can differ for the two different Py growths. Therefore, it would be interesting to study in future works more quantitatively on the relationship between induced surface effects and attenuated spin torque values in sputtered devices.

We have also measured the out-of-plane (OOP) angular dependence of symmetric and antisymmetric components of the lineshape that is given by the applied magnetic field angle θ. The motivation for such an experiment is that any new types of torques arising from interface effects other than that given by $\tau_\perp$ and $\tau_\parallel$ in Eq. (2) may be easier to elucidate in such an experiment.[30] The OOP field

Reuse of AIP Publishing content is subject to the terms at: https://publishing.aip.org/authors/rights-and-permissions. IP: 128.219.49.13 On: Fri, 04 Mar 2016 15:43:43

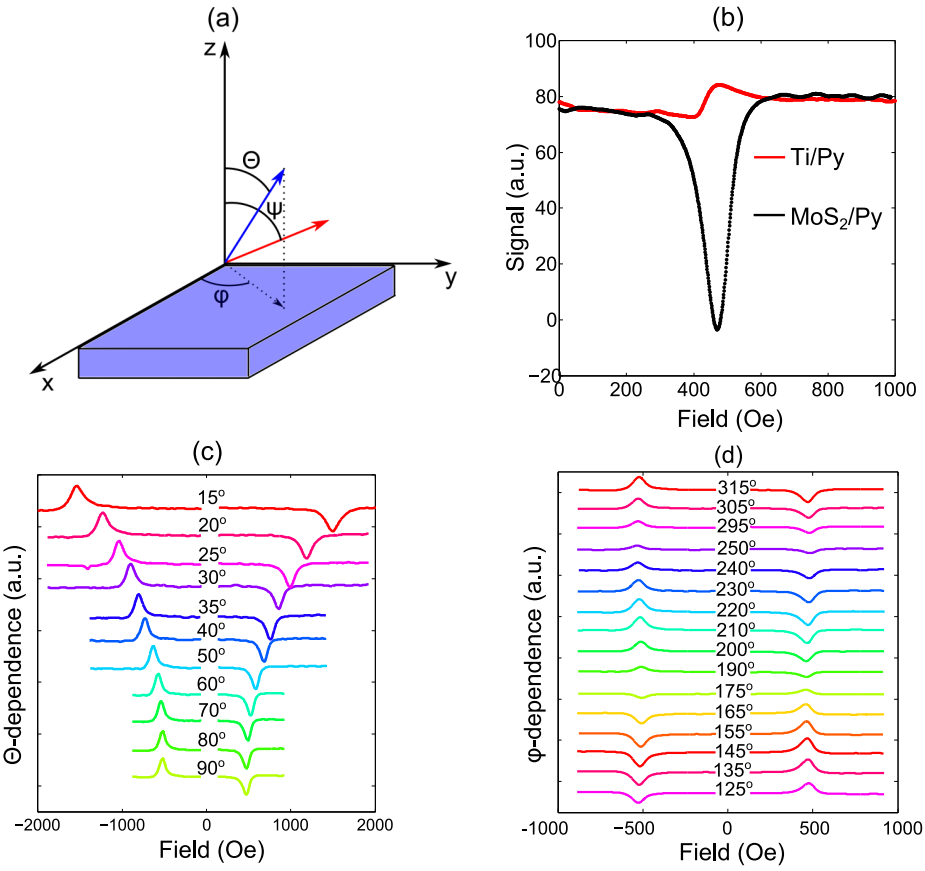

FIG. 5. Measurements with evaporated Py on MoS_2 and "normal-contacts." The field orientation and the device geometry is shown in (a). The applied field is described by the azimuthal angle ϕ and the polar angle θ. The magnetization is described by a different polar angle given as ψ. In (b), near $\phi = 45°$, a ST-FMR trace is shown for the MoS_2/Py bilayer vs a Ti/Py reference sample. The θ dependence at $\phi = 45°$ is shown in (c), while a large subset of the ϕ angular dependence is shown in (d).

data for θ in the range of 0°–75° are shown in Fig. 5(c); the data we are showing is for the magnetic field being swept from the positive to the negative direction. Generally, the magnitude of both the symmetric and antisymmetric components of the lineshape increases as θ decreases. The origin of this behavior may be from additional rectification occurring from the θ dependence of the magnetoresistance which was not previously measured. Another possibility is that the torques have a greater magnitude with decreasing θ. Towards this end, it is interesting to note that a strong dependence of spin-orbit torques as a function of θ has theoretically been predicted for the case of an interface with topological insulators.[31] Nevertheless, there is no clear observation suggesting additional out-of-plane torques in the system. Regarding the origin of the in-plane torques, it has been demonstrated that large spin torques can be induced by growing Py (or other ferromagnets) on oxides surface[32,33] with Rashba-type interface coupling, therefore it is plausible that the Py/MoS_2 interface alone can already give rise to these torques by symmetry-breaking of the Py. In addition, the strong Schottky barrier that might be developed at the Py/MoS_2 interface[34–36] can also give rise to a strong electric field, which further induces Rashba-type spin-splitting. Last but not least, the above-proposed interface spin-orbit effects may be convoluted by magnonic charge pumping effect,[37] taking advantage of not only the interfacial symmetry-breaking but also the intrinsic spin-orbit coupling of Py itself.[38] Finally, as shown in Fig. 6(d), there appears to be a hysteresis in the antisymmetric component of the lineshape compared to the symmetric component. Such hysteresis behavior is another strong evidence that speaks for the large symmetry-breaking of Py by its interfacing with MoS_2, which is also responsible for the large error bars in Fig. 6(b). Additional theoretical modeling regarding OOP ST-FMR experiments is required to further enhance the understanding of the current dataset.

Reuse of AIP Publishing content is subject to the terms at: https://publishing.aip.org/authors/rights-and-permissions. IP: 128.219.49.13 On: Fri, 04 Mar 2016 15:43:43

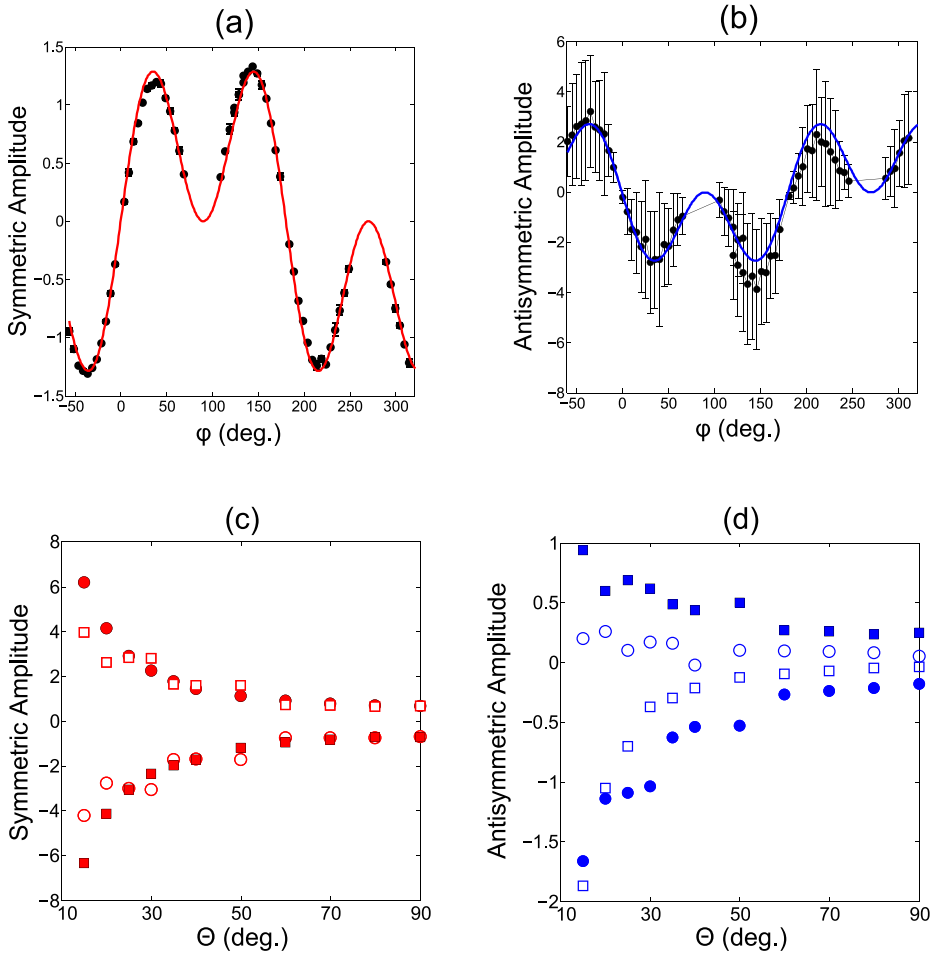

FIG. 6. Measurements with evaporated Py on MoS_2 and "normal-contacts." In (a) and (b) the symmetric and antisymmetric amplitude of the ST-FMR signal is shown as a function of ϕ. In (c) and (d) the symmetric and antisymmetric amplitude as a function of θ is plotted. Squares are data points that were extracted when the field was swept from positive to negative fields with the filled squares referring to the positive field amplitude and the unfilled squares referring to the negative field amplitudes. Circles correspond to measurements from negative to positive fields. The filled circles are on the negative field side while the unfilled are on the positive field side.

In summary, we report current induced spin torque resonance in permalloy(Py)/MoS_2 bilayers. Field-like and damping-like torques are induced by the MoS_2 layer which further excites the ferromagnetic resonance of Py. An analysis of the lineshapes with different measuring frequency, field orientation, and power is presented. The in-plane angular dependence suggests that a two torque model is required to explain the results. Specifically, a very large damping-like torque, relative to a field-like torque, is necessary to explain our data for both of the sample geometries. Out-of-plane angular measurements show an enhancement of the ST-FMR signal indicating a direction of future study. Our results suggest the potential of two-dimensional transition-metal dichalcogenide for the use of spin-orbitronics applications.

Z.Y. acknowledges the financial support from the Department of Electrical and Computer Engineering and College of Engineering at University of Illinois at Chicago, IGNITE Award, and Discovery Award for the CVD growth of the MoS_2 and optical characterizations. Work at Argonne, including device fabrication and magnetic and transport measurements, was supported by the U.S. Department of Energy, Office of Science, Materials Science and Engineering Division. Use of the Center for Nanoscale Materials for lithographic patterning was supported by the U.S. Department of Energy, Office of Science, and Basic Energy Sciences, under Contract No. DE-AC02-06CH11357.

Reuse of AIP Publishing content is subject to the terms at: https://publishing.aip.org/authors/rights-and-permissions. IP: 128.219.49.13 On: Fri, 04 Mar 2016 15:43:43

Work at ORNL is supported by the Division of Scientific User Facilities of the Office of Basic Energy Sciences, U.S. Department of Energy.

[1] A. Hoffmann and S. D. Bader, "Opportunities at the frontier of spintronics," Phys. Rev. Appl. **4**, 047001 (2015).
[2] L. Q. Liu *et al.*, "Spin torque switching with the giant spin Hall effect of tantalum," Science **336**, 555–558 (2012).
[3] L. Q. Liu, T. Moriyama, D. C. Ralph, and R. A. Buhrman, "Spin-torque ferromagnetic resonance induced by the spin Hall effect," Phys. Rev. Lett. **106**, 036601 (2011).
[4] W. Zhang *et al.*, "Spin pumping and inverse spin Hall effects—Insights for future spin-orbitronics (invited)," J. Appl. Phys. **117**, 172610 (2015).
[5] A. Hoffmann, "Spin Hall effects in metals," IEEE Trans. Magn. **49**, 5172 (2013).
[6] W. Zhang *et al.*, "Spin Hall effects in metallic antiferromagnets," Phys. Rev. Lett. **113**, 196602 (2014).
[7] W. Zhang *et al.*, "All-electrical manipulation of magnetization dynamics in a ferromagnet by antiferromagnets with anisotropic spin Hall effects," Phys. Rev. B **92**, 144405 (2015).
[8] A. Manchon, H. C. Koo, J. Nitta, S. M. Frolov, and R. A. Duine, "New perspectives for Rashba spin-orbit coupling," Nat. Mater. **14**, 871–882 (2015).
[9] V. M. Edelstein, "Spin polarization of conduction electrons induced by electric current in two-dimensional asymmetric electron systems," Solid State Commun. **73**, 233–235 (1990).
[10] A. Chernyshov *et al.*, "Evidence for reversible control of magnetization in a ferromagnetic material by means of spin-orbit magnetic field," Nat. Phys. **5**, 656–659 (2009).
[11] J. C. Rojas-Sanchez *et al.*, "Spin-to-charge conversion using Rashba coupling at the interface between non-magnetic materials," Nat. Commun. **4**, 2944 (2013).
[12] K. Chen and S. Zhang, "Spin pumping in the presence of spin-orbit coupling," Phys. Rev. Lett. **114**, 126602 (2015).
[13] W. Zhang, M. B. Jungfleisch, W. Jiang, J. E. Pearson, and A. Hoffmann, "Spin pumping and inverse Rashba-Edelstein effect in NiFe/Ag/Bi and NiFe/Ag/Sb," J. Appl. Phys. **117**, 17C727 (2015).
[14] M. B. Jungfleisch, W. Zhang, J. Sklenar, W. Jiang, J. E. Pearson, J. B. Ketterson, and A. Hoffmann, "Interface-driven spin-torque ferromagnetic resonance by Rashba coupling at the interface between non-magnetic materials," e-print arXiv:1508.01410.
[15] X. Fan, H. Celik, J. Wu, C. Ni, K. J. Lee, V. O. Lorenz, and J. Q. Xiao, "Quantifying interface and bulk contributions to spin-orbit torque in magnetic bilayers," Nat. Commun. **5**, 3042 (2014).
[16] J. B. S. Mendes *et al.*, "Spin-current to charge-current conversion and magnetoresistance in a hybrid structure of graphene and yttrium iron garnet," Phys. Rev. Lett. **115**, 226601 (2015).
[17] A. R. Mellnik *et al.*, "Spin-transfer torque generated by a topological insulator," Nature **511**, 449–451 (2014).
[18] Y. Fan *et al.*, "Magnetization switching through giant spin-orbit torque in a magnetically doped topological insulator heterostructure," Nat. Mater. **13**, 699–704 (2014).
[19] D. Xiao, G. B. Liu, W. Feng, X. Xu, and Y. Wang, "Coupled spin and valley physics in monolayers of MoS2 and other group-VI dichalcogenides," Phys. Rev. Lett. **108**, 196802 (2012).
[20] C. Cheng *et al.*, "Direct observation of spin-to-charge conversion in MoS2 monolayer with spin pumping," e-print arXiv:1510.03451.
[21] H. Yuan *et al.*, "Zeeman-type spin splitting controlled by an electric field," Nat. Phys. **9**, 563–569 (2013).
[22] A. T. Neal, Y. Du, H. Liu, and P. D. Ye, "Two-dimensional $TaSe_2$ metallic crystals: Spin-orbit scattering length and breakdown current density," ACS Nano **8**, 9137–9142 (2014).
[23] A. Kormanyos *et al.*, "Spin-orbit coupling, quantum dots, and qubits in monolayer transition metal dichalcogenides," Phys. Rev. X **4**, 011034 (2014).
[24] D. Culcer and R. Winkler, "Generation of spin currents and spin densities in systems with reduced symmetry," Phys. Rev. Lett. **99**, 226601 (2007).
[25] H. J. Juretschke, "Electromagnetic theory of dc effects in ferromagnetic resonance," J. Appl. Phys. **31**, 1401 (1960).
[26] H. J. Juretschke, "dc detection of spin resonance in thin metallic films," J. Appl. Phys. **34**, 1223 (1963).
[27] P. K. Chow *et al.*, "Defect-induced photoluminescence in monolayer semiconducting transition metal dichalcogenides," ACS Nano **9**, 1520 (2015).
[28] M. Harder, Z. X. Cao, Y. S. Gui, X. L. Fan, and C. -M. Hu, "Analysis of the line shape of electrically detected ferromagnetic resonance," Phys. Rev. B **84**, 054423 (2011).
[29] T. Chiba, M. Schreier, G. E. W. Bauer, and S. Takahashi, "Current-induced spin torque resonance of magnetic insulators affected by field-like spin-orbit torques and out-of-plane magnetizations," J. Appl. Phys. **117**, 17C715 (2015).
[30] J. Sklenar, "Control of ferromagnetic resonance in thin films through nanostructuring and interfacial torques," Ph.D. thesis, Northwestern University, 2015.
[31] P. B. Ndiaye, C. A. Akosa, M. H. Fischer, A. Vaezi, E. -A. Kim, and A. Manchon, "Dirac spin-orbit torques at the surface of topological insulators," e-print arXiv:1509.06929.
[32] A. Tsukahara, Y. Ando, Y. Kitamura, H. Emoto, E. Shikoh, M. P. Delmo, T. Shinjo, and M. Shiraishi, "Self-induced inverse spin Hall effect in permalloy at room temperature," Phys. Rev. B **89**, 235317 (2014).
[33] M. Akyol, J. G. Alzate, G. Yu, P. Upadhyaya, K. L. Wong, A. Ekicibil, P. K. Amiri, and K. L. Wang, "Effect of the oxide layer on current-induced spin-orbit torques in Hf/CoFeB/MgO and Hf/CoFeB/TaO_x structures," Appl. Phys. Lett. **106**, 032406 (2015).
[34] W. Y. Wang *et al.*, "Spin-valve effect in NiFe/MoS2/NiFe junctions," Nano Lett. **15**, 5261 (2015).
[35] S. Xu *et al.*, "High-quality BN/WSe2/BN heterostructure and its quantum oscillations," e-print arXiv:1503.08427.
[36] X. Cui *et al.*, "Multi-terminal transport measurements of MoS_2 using a van der Waals heterostructure device platform," Nat. Nanotechnol. **10**, 534 (2015).
[37] C. Ciccarelli, K. M. D. Hals, A. Irvine, V. Novak, Y. Tserkovnyak, H. Kurebayashi, A. Brataas, and A. Ferguson, "Magnonic charge pumping via spin-orbit coupling," Nat. Nanotechnol. **10**, 50 (2015).
[38] A. Azevedo *et al.*, "Electrical detection of ferromagnetic resonance in single layers of permalloy: Evidence of magnonic charge pumping," Phys. Rev. B **92**, 024402 (2015).

Reuse of AIP Publishing content is subject to the terms at: https://publishing.aip.org/authors/rights-and-permissions. IP: 128.219.49.13 On: Fri, 04 Mar 2016 15:43:43